Nanoscale

Accepted Manuscript

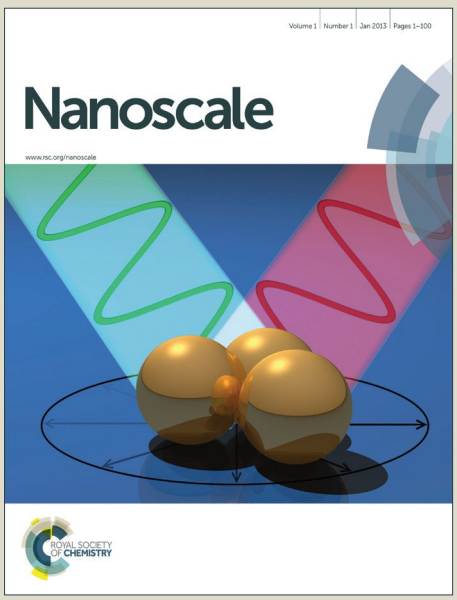

ROYAL SOCIETY OF CHEMISTRY

www.rsc.org/nanoscale

Reduction of interfacial friction in commensurate graphene/h-BN heterostructures by surface functionalization

Yufeng Guo*, Jiapeng Qiu and Wanlin Guo

State Key Laboratory of Mechanics and Control of Mechanical Structures and MOE Key Laboratory for Intelligent Nano Materials and Devices, Institute of Nanoscience, Nanjing University of Aeronautics and Astronautics, Nanjing, 210016, China

Abstract:

To reduce interfacial friction in two-dimensional layered materials of commensurate stacking is important for their application in nanoelectromechanical systems. Our first-principles calculations about the sliding energy corrugation and friction in the interfaces of commensurate fluorinated-graphene/h-BN and oxidized-graphene/h-BN heterostructures show that the sliding energy barriers and shear strengths for these heterostructures are approximately decreased to 50% of that in commensurate graphene/h-BN. The adsorbed F and O atoms significantly suppress the interlayer electrostatic and van der Waals energy corrugations by modifying the geometry and charge redistribution of the graphene layers. Our empirical registry index models further reveal the difference between the roles of the F and O atoms in affecting the sliding energy landscapes, which are also utilized to predict the interlayer superlubricity in large-scale oxidized-graphene/h-BN system. Surface functionalization is a valid way to control and reduce the interlayer friction in commensurate graphene/h-BN heterostructure.

*Corresponding author. Tel.: +86 25 84890513 Fax: +86 25 84895827. E-mail address: yfguo@nuaa.edu.cn.

1. Introduction

Understanding interfacial tribology is essential for actual application of two dimensional (2D) layered materials that are held by weak interlayer van der Waals (vdW) forces in functional devices and nanoelectromechanical systems (NEMS). An important type of solid lubricants is homogenous layered materials such as graphite, hexagonal boron nitride (h-BN), and 2H-molybdenum disulphide [1-5]. The interface friction and interlayer potential landscape of homogenous 2D layered materials have been extensively studied by experimental and theoretical methods [6-20]. Recently, the wearless friction or superlubricity was observed in layered graphene system of incommensurate stacking [6]. However, this ultra-low interlayer friction strongly depends on the degree of commensurability between the lattices of graphene layers, and will disappear when one of the sliding surfaces is rotated by a certain angle or the interface transforms from incommensurate into commensurate. On the other hand, artificial heterogeneous layered materials, which are stacks of different 2D crystals, have attracted great scientific interests as novel properties coming from the combination of unique physical properties of each individual layer and all their different advantages can be properly utilized [21,22]. Due to lattice mismatch between 2D crystals and the presence of moiré patterns, layered heterostructures often exhibit incommensurate interfaces, which remarkably reduce the interlayer friction and sliding resistance [23-25] because of changes of the interatomic distances and interlayer interactions. A recent experimental work [26] reported a commensurate–incommensurate transition for graphene on top of h-BN when the rotation angle of graphene reaching a

critical value, and this leads to an alteration in the electronic and optical properties of graphene/h-BN heterostructures. Another theoretical study [27] further revealed the important role of the ratio between carbon-boron and carbon-nitrogen interactions in the graphene/h-BN heterostructures determining the strain distribution in the moiré pattern.

For vdW layered materials, the commensurate stacking is energetically more favorable than the incommensurate stacking [28]. To lower the interlayer friction in commensurate interface is an intriguing aspect in nanofabrication of vdW layered materials and control of their tribology properties. By using h-BN layers as flat dielectric substrates, graphene/h-BN heterostructures exhibit much higher carrier mobility and current density compared with SiO_2 substrates [29-31], which has led to the realization of graphene electronic devices with better performance. Experiments have shown that the stacking of graphene on h-BN could be the commensurate state because of very slight lattice mismatch between them [26]. Graphene and h-BN have high surface-to-volume ratios and their surfaces are easily decorated by other atoms, molecules and radicals. Moreover, surface functionalization such as fluorination and oxidation is an important route to change and monitor the mechanical and physical properties of 2D crystals [32-36]. Further study about the effects of surface functionalization on the interlayer interaction and friction of graphene/h-BN system is necessary for the development of layered heterostructures based on graphene and graphene-like 2D materials.

In this study, we have investigated the sliding energy corrugation and friction in the

interfaces of commensurate fluorinated-graphene/h-BN and oxidized-graphene/h-BN heterostructures by first-principles calculations. From the calculated potential energy surfaces (PESs), the sliding energy barriers and shear strengths for these fluorinated and oxidized heterostructures are approximately reduced to 50% of that in commensurate graphene/h-BN. The reduction in the interlayer friction is attributed to fluorination and oxidation induced charge redistribution and change of vdW interaction. Furthermore, the registry index models are developed to describe the role of F and O atoms in the interlayer friction and provide a quantitative way to predict the sliding energy landscape of large-scale fluorinated or oxidized graphene/h-BN system.

2. Model and Method

In our model, two types of heterostructures were established in the rhombus unit cells ($a_1 = a_2 = 10.096$ Å) in which a 4 × 4 graphene monolayer (32 atoms) was placed on a 4 × 4 h-BN monolayer (32 atoms) with the AB stacking and the top surface of the graphene layer was fully decorated by 16 F or O atoms, as shown in Fig. 1 and 2. The initial lengths of the B-N bond and C-C bond are 1.45Å and 1.42 Å, respectively, and there is a vacuum region larger than 2.5 nm in the direction (the z direction) perpendicular to the heterostructure planes. All computations were performed within the framework of density-functional theory (DFT) as implemented in the VASP code by using the projector augmented wave method with the Perdew-Burke-Ernzerhof (PBE) exchange-correlation functional [37-39]. The influence of vdW interactions was considered by using a modified version of vdW-DF, referred to as "optB86b-vdW," in

which the revPBE exchange functional of the original vdW-DF of Dion *et al.*, is replaced with the optB86b exchange functional to yield more accurate equilibrium interatomic distances and energies for a wide range of systems [40, 41]. Those systems were relaxed by using a conjugate-gradient algorithm until the force on each atom is less than 0.1 eV/nm.

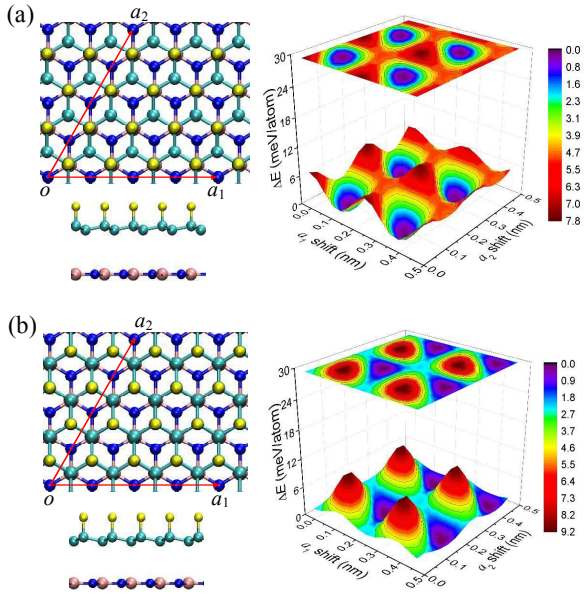

Fig. 1 Initial atomic configurations of fluorinated-graphene/h-BN heterostructures. (a) F-C bonds on the top of B atoms (*a*-type) and (b) F-C bonds on the hollow sites of the h-BN plane (*b*-type), and the corresponding PESs when the fluorinated graphene layers are sliding with respect to the bottom h-BN layers with fixed interlayer distances. The yellow, cyan, blue and pink dots are F, C, N and B atoms, respectively.

For fluorinated-graphene/h-BN, there are two stable adsorption sites for the F atoms (Fig. 1): one is the F-C bonds on the top of B atoms (*a*-type) with an interlayer

distance of 0.332 nm and another is the F-C bonds on the hollow sites of the h-BN plane (*b*-type) with an interlayer distance of 0.323 nm. There are also two stable adsorption sites for the O atoms (Fig. 2): one is the O on the C-C bond 30^{o} to the a_1 axis (*a*-type)with an interlayer distance of 0.327 nm and another is the O on the C-C bond vertical to the a_1 axis (*b*-type) with an interlayer distance of 0.324 nm. To match with the h-BN layers, the lattice constants of the fluorinated and oxidized graphene layers are compressed 0.078% and 5.25%, respectively. As a result, the interfaces at the fluorinated-graphene/h-BN and oxidized-graphene/h-BN heterostructures can still be considered to be commensurate. After structural relaxation, the fluorinated and oxidized graphene layers are translated to relatively different positions in the a_1-a_2 plane where the nearest translational positions are separated by 0.036 nm, and the interlayer distances with respective to the bottom h-BN layers are fixed to be the initial equilibrium interlayer distances. At different sliding positions, the three coordinates of each atom are fixed, and the computations with an energy cutoff of 500 eV and special *k* points sampled on a 6×6×1 Monkhorst-Pack mesh [42] are employed to calculate the total energy. The corresponding PESs for interlayer sliding are constructed and obtained by the deviation between the calculated total energy at different positions and the lowest energy of the system. As the force at the *z* direction (normal direction) of each atom is hard to be modulated to reach a desired normal force in the DFT calculations, we construct the PES by fixing interlayer distance that has been adopted by previous theoretical studies on interlayer sliding [11, 13, 16, 24, 25]. However, for comparison, we have also studied the case of normal force

approximately being zero where the *z* coordinate of each atom is fully relaxed but the *x* and *y* coordinates are fixed at different sliding positions.

3. Results and Discussion

One-side fluorination of graphene leads to a corrugated structure, as shown in Fig. 1, where the C atoms bonding with F atoms are lifted up. The formation energies E_f for the *a*-type and *b*-type fluorinated heterostructures are 0.96 and 0.79 eV, respectively, which are calculated by $E_f = E_t - E_{gra/bn} - 8E_{f2}$ (E_t is the total energy, $E_{gra/bn}$ is the energy of the graphene/h-BN heterostructure and E_{f2} is the energy of a F_2 molecule). The fluorination of the graphene/h-BN is endothermic, and the *b*-type is more stable than the *a*-type because of a lower total energy. From the PES of the *a*-type, the maximum energy barrier (the difference between ΔE_{max} and ΔE_{min}) is 7.8 meV per C atom when the fluorinated graphene layer slides relatively to the lower h-BN layer. While the maximum energy barrier for the *b*-type increases to 9.2 meV/atom. According to the maximum static resistance force f_{mr} acting on the fluorinated graphene layer during the sliding process, the interlayer shear strength τ can be estimated by $\tau = |\frac{f_{mr}}{A}|$, here A is the area of the unit cell. The corresponding shear strengths for the *a*-type and *b*-type fluorinated graphene layers are 0.488 and 0.625 GPa.

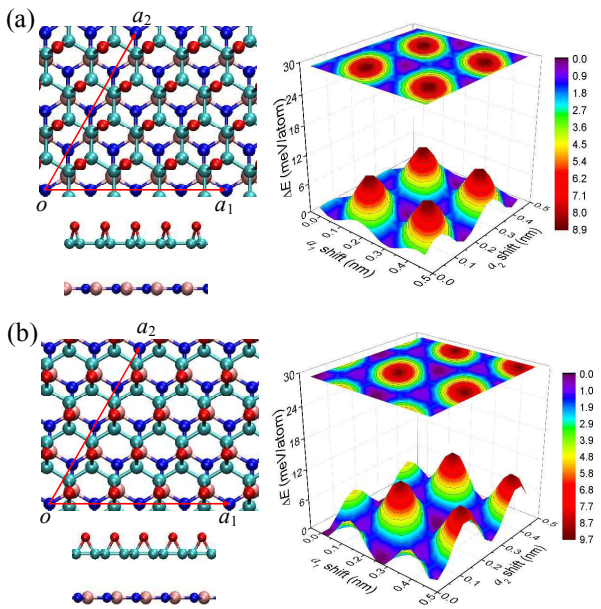

Fig. 2 Initial atomic configurations of oxidized-graphene/h-BN heterostructures. (a) O on the C-C bond 30^o to the a_1 axis (*a*-type) and (b) O on the C-C bond vertical to the a_1 axis (*b*-type), and the corresponding PESs when the oxidized graphene layers are sliding with respect to the bottom h-BN layers with fixed interlayer distances. The red, cyan, blue and pink dots are O, C, N and B atoms, respectively.

Different from the fluorinated graphene, the plane of graphene still remains flat after oxidation, as shown in Fig. 2. By the same calculation method of fluorination, the formation energies E_f for the *a*-type and *b*-type oxidized heterostructures are 0.77 and 0.70 eV, respectively, which indicates the endothermic oxidation process. The maximum energy barriers of the *a*-type and the *b*-type are 8.9 and 9.7 meV/atom and the shear strengths are 0.611 and 0.704 GPa, respectively, when the oxidized graphene layers slide relatively to the lower h-BN layers. The interlayer energy corrugations

and shear strengths in the oxidized graphene/h-BN heterostructures are larger than that in the fluorinated heterostructures. We have also calculated the sliding PES of the AB stacking graphene/h-BN (Fig. 3), and the obtained maximum energy barrier and shear strength are 16.4 meV and 1.121 GPa, respectively. Compared with the graphene/h-BN system, the energy corrugations in the *a*-type and *b*-type fluorinated heterostructures are reduced by 52.4% and 44.0%, respectively, and for oxidized heterostructures the energy corrugations in the *a*-type and *b*-type are reduced by 46.0% and 41.0%, respectively. As proposed by Prantl-Tomlinson model, the energy corrugation in the PES and the stiffness of sliding layer are important factors for predicting actual interlayer friction properties [43, 44]. Higher energy corrugation and smaller stiffness will lead to higher interlayer friction. According to the previous study [11], the stiffness K of the sliding layer can be approximately estimated by $K = \partial^2 E/\partial s^2$, here E is the potential energy field of interlayer interaction, which can be deduced by the calculated PES, and s is the relative lateral displacement of the sliding layer. Our calculations show that both the stiffness of fluorinated and oxidized graphene are slightly larger than that of pure graphene. Those results clearly demonstrate that the fluorination and oxidation are valid ways to reduce the interlayer friction in commensurate graphene/h-BN heterostructure.

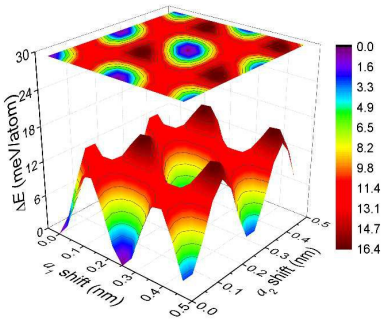

Fig. 3 PES for a graphene layer sliding on an h-BN layer with a fixed interlayer distance of 0.326 nm.

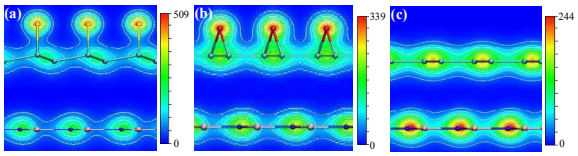

Fig. 4 2D projections of charge densities (in units of e/Å^3) of the (a) *a*-type fluorinated, (b) *a*-type oxidized and (c) pure graphene/h-BN heterostructures. The dot denotation is the same as that in Fig. 1 and 2.

To understand the roles of the adsorbed F and O atoms, we plot the charge density distributions of the fluorinated, oxidized and pure graphene/h-BN heterostructures in Fig. 4. It can be seen from the magnitudes of charge accumulations that the F, O and N atoms carry negative charges and B atoms carry positive charges, and the fluorination and oxidation slightly influence the charge distribution in the h-BN layer. The charge properties are slightly changed when the graphene layer slides with respect to the bottom h-BN layer. For the *b*-type heterostructures, the charge density distributions are similar to that of the *a*-type. The main factors that govern energy corrugation in such layered system are electrostatic and dispersion (or vdW)

interactions. In contrast to the graphene/h-BN, the coupling of the repulsive coulomb interaction between the negative F or O atoms and negative N atoms with the attractive coulomb interaction between the negative F or O atoms and positive B atoms weakens the interlayer energy corrugation. Moreover, the interlayer vdW energy corrugations are also weakened by the fluorination and oxidation, as shown by Fig. 5. Due to the increasing in the interlayer distance of the C atoms bonding with the F atoms to the h-BN layer, the vdW energy corrugations in the fluorinated systems are lower than that in the oxidized systems. Both the electrostatic and vdW energy corrugations are decreased by fluorination and oxidation, which consequently leads to the reduction of interlayer friction.

Besides the case of fixed interlayer distance, we have also studied the interlayer energy corrugations of pure, *a*-type fluorinated and *a*-type oxidized graphene/h-BN heterostructures in which their normal forces are approximately zero realizing by relaxation of the *z* coordinates of atoms. The obtained PESs of the three cases are very similar to that of the corresponding heterostructures of fixed interlayer distances, and the maximum energy barriers for the three cases are 11.1, 8.8 and 8.4 meV/atom, respectively. Coinciding with the results shown in Fig. 1 to 3, fluorination and oxidation significantly reduce the interlayer sliding friction when the normal force is zero. Moreover, the effects of other oxidation manner where the surface of graphene is uniformly decorated by four O-H radicals on the interlayer sliding friction has been investigated by the same method with normal force being zero. Here the O-H radicals adsorb on the C atoms and are separated by 0.505 nm. The calculated maximum

energy barrier is only 6.6 meV/atom, just 59% of that in pure graphene/h-BN heterostructure (11.1 meV/atom). This means that the adsorption of O-H radical can also reduce the interlayer sliding friction.

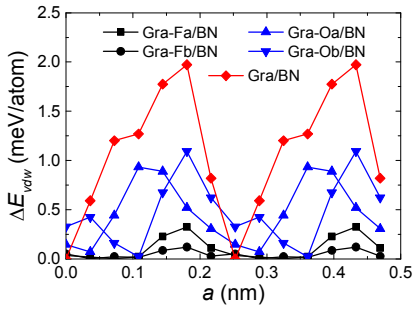

Fig. 5 Energy corrugation profiles of the van der Waals energy for the fluorinated, oxidized and pure graphene layers sliding on the h-BN layers with the straight paths crossing the maximum and minimum values of Δ*E*.

As the capability and scale of the present DFT calculations are limited, the registry index (RI) methods that quantify the registry matching using basic geometric considerations are recently developed to provide qualitative explanations for the interlayer sliding energy landscapes of layered vdW materials [13-15]. The main contribution to the corrugation energy comes from the electrostatic interactions between the atomic sites, as shown in Fig. 4. Each atom in the unit cell can be ascribed to a circle centered on its position, and then the RI based on the overlap area of circle projection between the atoms in the top and bottom layers at different sliding positions are used to mimic the sliding energy corrugation [13]. According to the definition of RI and our DFT results, we establish the RI models of the fluorinated and oxidized heterostructures to further elucidate the atomistic mechanisms of surface

fluorination and oxidation on the interlayer friction. For the *a*-type fluorinated-graphene/h-BN, the RI is defined as

$$RI = \frac{[(S_{C1B} - S_{C1B}^{L}) - (S_{C1N} - S_{C1N}^{L})] + [(S_{C2B} - S_{C2B}^{L}) - (S_{C2N} - S_{C2N}^{L})] + [(S_{FN} - S_{FN}^{L}) + (S_{FB} - S_{FB}^{L})]}{[(S_{C1B}^{H} - S_{C1B}^{L}) - (S_{C1N}^{H} - S_{C1N}^{L})] + [(S_{C2B}^{H} - S_{C2B}^{L}) - (S_{C2N}^{H} - S_{C2N}^{L})] + [(S_{FN}^{H} - S_{FN}^{L}) + (S_{FB}^{H} - S_{FB}^{L})]}.$$

Here S_{C1B}^{H}, S_{C1N}^{H}, S_{C2B}^{H}, S_{C2N}^{H}, S_{FB}^{H} and S_{FN}^{H} are the overlap areas of atomic circle projection between the low C atoms in the top layer and B atoms in the bottom layer, the low C atoms and N atoms, the high C atoms and B atoms, the high C atoms and N atoms, the F atoms and B atoms, the F atoms and N atoms, respectively, when the whole system is at the highest energy state indicated by the DFT results. S_{C1B}^{L}, S_{C1N}^{L}, S_{C2B}^{L}, S_{C2N}^{L}, S_{FB}^{L} and S_{FN}^{L} are the projected circle overlaps at the lowest energy state, as shown in Fig. 6 (a). S_{C1B}, S_{C1N}, S_{C2B}, S_{C2N}, S_{FB} and S_{FN} are the projected overlaps of those atoms where the fluorinated graphene layer translates to any position. The atomic radii *r* defining the circle area by πr^2 for the C, B, N and F atoms are 0.91, 0.86, 0.71 and 0.74Å, respectively. The mapped RI as a function of the lateral interlayer shifts locates at the range from 0 to 1 and its profile is well consistent with the DFT results, as shown in Fig. 6 (a). So the RI model can qualitatively describe the interlayer energy corrugation of the fluorinated heterostructure. For the *a*-type oxidized-graphene/h-BN, the RI is expressed as

$$RI = \frac{[(S_{CB} - S_{CB}^{L}) + (S_{CN} - S_{CN}^{L})] + 0.5[(S_{ON} - S_{ON}^{L}) - (S_{OB} - S_{OB}^{L})]}{[(S_{CB}^{H} - S_{CB}^{L}) + (S_{CN}^{H} - S_{CN}^{L})] + 0.5[(S_{ON}^{H} - S_{ON}^{L}) - (S_{OB}^{H} - S_{OB}^{L})]}.$$

Here the definition of each parameter is similar to that for the fluorinated case except that all C atoms are in the same plane, and the atomic radius of the O atoms is 0.82Å. The obtained RI profile shown in Fig. 6 (b) is also consistent with the DFT results. In

contrast to the fluorination RI model, there is a coefficient of 0.5 for the items of O atoms in the oxidation RI model, indicating a smaller influence from the O atoms. When this coefficient equals to zero, the oxidation RI equation completely becomes the RI of the pure graphene/h-BN system [24]. This is because that the adsorbed F atoms lead to a corrugated graphene layer, while the C plane still remains flat after oxidation. Therefore, higher sliding energy barrier and shear strength in the oxidized-graphene/h-BN can be qualitatively explained by the difference between the fluorination and oxidation RI models. Similar trends have also been observed in the RI models of the b-type fluorinated and oxidized graphene/h-BN heterostructures.

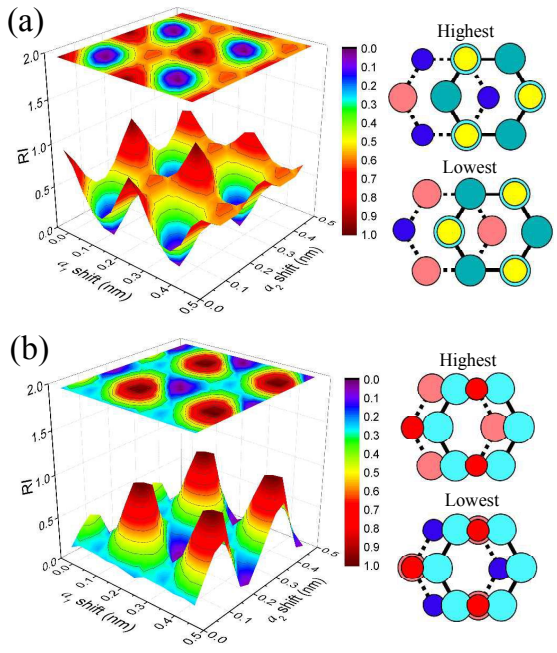

Fig. 6 The profiles of the registry index for (a) *a*-type fluorinated and (b) *a*-type oxidized graphene/h-BN, and the corresponding atomic circle configuration and superposition at the highest and lowest total energies. The red, cyan, blue and pink circles are O, C, N and B atoms, respectively. The dark cyan and cyan

circles in (a) are the high and low C layers to the bottom h-BN layer, respectively.

The mismatch between the lattice constants of the fluorinated graphene and h-BN is only 0.078%. Such slight difference means that the interlayer stacking of the fluorinated graphene and h-BN layers at actual situation can be considered as commensurate if no rotation occurs. However, the lattice difference between the oxidized graphene and h-BN is 5.25%, and thus the actual interlayer stacking without any constraint should be incommensurate. Here we have used the oxidation RI model to predict the interlayer friction of the oxidized-graphene/h-BN of incommensurate stacking. As shown by the inset of Fig. 7, a one-side oxidized graphene flake of 4.796 nm × 8.306 nm is placed on an h-BN layer. The flake is first rotated by an angle and slides along different directions in the *xy* plane with a fixed interlayer distance of 0.324 nm. Then the corresponding RI at different positions is calculated by our model. The maximum RI for a rotation angle is selected out and given in Figure 7, in which all RI are lower than 0.42. Smaller maximum RIs indicate lower interlayer energy corrugations and the interlayer sliding in oxidized-graphene/h-BN heterostructure should be superlubricant. This is consistent with other theoretical prediction about interlayer friction in the incommensurate system [23, 24].

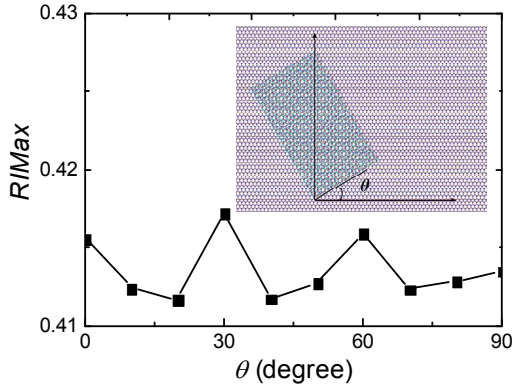

Fig. 7 The maximum registry index of an oxidized graphene flake sliding on the single-layer h-BN substrate when the graphene flake is rotated by different angles. The inset shows the rotated structure of the oxidized graphene on the h-BN layer.

4. Conclusion

In summary, our first-principles calculations show that surface fluorination and oxidation could remarkably reduce the interfacial friction in commensurate graphene/h-BN heterostructures, as the adsorbed F and O atoms significantly suppress the interlayer electrostatic and vdW energy corrugations. The established empirical registry index models further reveal the difference between the roles of the F and O atoms in affecting the sliding energy landscapes, which are also utilized to predict the interlayer superlubricity in large-scale oxidized-graphene/h-BN system. These results provide some insights into using surface functionalization to control and reduce interlayer friction in commensurate 2D layered materials.

Acknowledgements

This work is supported the NSF (11072109, 11472131), the Program for New Century Excellent Talents in University (NCET-13-0855), the Jiangsu NSF (BK20131356), the 973 Program (2013CB932604, 2012CB933403), the Fundamental Research Funds for the Central Universities (NE2012005, NJ20150048, NJ20150048, INMD-2015M02) of China, and the Research Fund of State Key Laboratory of Mechanics and Control of Mechanical Structures (Nanjing University of Aeronautics and Astronautics) (0413G01, MCMS-0414G01), a Project Funded by the Priority Academic Program Development of Jiangsu Higher Education Institutions, and sponsored by Qing Lan Project.

References

1. B. K. Yen, B. E. Schwickert and M. F.Toney, *Appl. Phys. Lett.*, 2004, **84**, 4702.
2. L. Rapoport, N. Fleischer and R. Tenne, *Adv. Mater*, 2003, **15**, 651.
3. C. Lee, Q. Li, W. Kalb, X.-Z. Liu, H. Berger, R. W. Carpick and J. Hone, *Science*, 2010, **328**, 76.
4. C. Donnet and A. Erdemir, *Surf. Coat. Technol*, 2004, **180**, 76.
5. S. Brown, J. L. Musfeldt, I. Mihut, J. B. Betts, A. Migliori, A. Zak and R.Tenne, *Nano Lett.*, 2007, **7**, 2365.
6. M. Dienwiebel, G. S. Verhoeven, N. Pradeep, J. W. M.Frenken, J. A. Heimberg and H. W. Zandbergen, *Phys. Rev. Lett.*, 2004, **92**, 126101.
7. Y. F. Guo, W. L. Guo and C. F. Chen, *Phys. Rev. B*, 2007, **76**, 155429.
8. Q. S. Zheng, B. Jiang, S. Liu, Y. Weng, L. Lu, Q. Xue, J. Zhu, Q. Jiang, S. Wang

and L. Peng, *Phys. Rev. Lett.*, 2008, **100**, 067205.

9. Z. Liu, J. Yang, F. Grey, J. Z. Liu, Y. Liu, Y. Wang, Y. Yang, Y. Cheng and Q. Zheng, *Phys. Rev. Lett.*, 2012, **108**, 205503.
10. A. Smolyanitsky, J. P. Killgore and V. K. Tewary, *Phys. Rev. B*, 2012, **85**, 035412.
11. L. Xu, T. B. Ma, Y. Z. Hu and H. Wang, *Nanotechnology*, 2011, **22**, 285708.
12. X. Feng, S. Kwon, J. Y. Park and M. Salmeron, *ACS Nano*, 2013, **7**, 1718.
13. N. Marom, J. Bernstein, J. Garel, A. Tkatchenko, E. Joselevich, L. Kronik and O. Hod, *Phys. Rev. Lett.*, 2010, **105**, 046801.
14. A. Blumberg, U. Keshet, I. Zaltsman and O. Hod, *J. Phys. Chem. Lett.*, 2012, **3**, 1936.
15. O. Hod, *Phys. Rev. B*, 2012, **86**, 075444.
16. G. Constantinescu, A. Kuc and T. Heine, *Phys. Rev. Lett.*, 2013, **111**, 036104.
17. G. Levita, A. Cavaleiro, E. Molinari, T. Polcar, and M. C. Righi, *J. Phys. Chem. C.*, 2014, **118**, 13809.
18. J. P. Oviedo, K. C. Santosh, N. Lu, J. G. Wang, K. Cho, R. M. Wallace and M. J. Kim, *ACS Nano*, 2015, **9**, 1543.
19. E. Koren, E. Lörtscher, C. Rawlings, A. W. Knoll and U. Duerig, *Science*, 2015, **348**, 679.
20. W. Gao and A. Tkatchenko, *Phys. Rev. Lett.*, 2015, **114**, 096101.
21. A. K. Geim and I. V. Grigorieva, *Nature*, 2013, **499**, 419.
22. E. Gibney, *Nature*, 2015, **522**, 274.
23. L. F. Wang, T. B. Ma, Y. Z. Hu, Q. S. Zheng, H. Wang and J. B. Luo,

Nanotechnology, 2014, **25**, 385701.

24. I. Leven, D. Krepel, O. Shemesh and O. Hod, *J. Phys. Chem. Lett.*, 2013, **4**, 115.
25. X. Y. Zhao, L. Y. Li and M. W. Zhao, *J. Phys.: Condens. Matter*, 2014, **26**, 095002.
26. C. R.Woods, L. Britnell, A. Eckmann, R. S. Ma, J. C. Lu, H. M. Guo, X. Lin, G. L. Yu, Y. Cao, R. V. Gorbachev, A. V. Kretinin1, J. Park1, L. A. Ponomarenko1, M. I. Katsnelson, Yu. N. Gornostyrev, K.Watanabe, T. Taniguchi, C. Casiraghi, H-J. Gao, A. K. Geim and K. S. Novoselov, *Nat. Phys.*, 2014, **10**, 451.
27. M. M. van Wijk, A. Schuring, M. I. Katsnelson, and A. Fasolino, *Phys. Rev. Lett.*, 2014, **113**, 135504.
28. A. E. Filippov, M. Dienwiebel, J. W. M. Frenken, J. Klafter and M. Urbakh, *Phys. Rev. Lett.*, 2008, **100**, 046102.
29. S. D. Sarma and E. H. Hwang, *Phys. Rev. B*, 2011, **83**, 121405.
30. J. Xue, J. S. Yamagishi, D. Bulmash, P. Jacquod, A. Deshpande, K. Watanabe, T. Taniguchi, P. J. Herrero and B. J. LeRoy, *Nat. Mater.*, 2011, **10**, 282.
31. E. Kim, T. Yu, E. S. Song and B. Yu, *Appl. Phys. Lett.*, 2011, **98**, 262103.
32. Z. H. Zhang, X. C. Zeng and W. L. Guo, *J. Am. Chem. Soc.*, 2011, **133**, 14831.
33. Y. Zhao, X. Wu, J. Yang and X. C. Zeng, *Phys. Chem. Chem. Phys.*, 2012, **14**, 5545.
34. B. Huang, H. Xiang, J. Yu and S. H. Wei, *Phys. Rev. lett.*, 2012, **108**, 206802.
35. M. Du, X. Li, A. Wang, Y. Wu, X. Hao and M. Zhao, *Angew. Chem. Int. Ed.*, 2014, **53**, 3645.

36. Y. F. Guo and W. L. Guo, *Nanoscale*, 2014, **6**, 3731.

37. P. E. Blochl, *Phys. Rev. B*, 1994, **50**, 17953.

38. G. Kresse and D. Joubert, *Phys. Rev. B*, 1999, **59**, 1758.

39. J. P. Perdew, K. Burke and M. Ernzerhof, *Phys. Rev. Lett.*, 1996, **77**, 3865.

40. J. Klimes, D. R. Bowler and A. Michelides, *J. Phys.: Cond Matt.*, 2010, **22**, 022201.

41. J. Klimes, D. R. Bowler and A. Michelides, *Phys. Rev. B*, 2011, **83**, 195131.

42. H. J. Monkhorst and J. D. Pack, *Phys. Rev. B*, 1976, **13**, 5188.

43. A. Vanossi, N. Manini, M. Urbakh, S. Zapperi and E. Tosatti, *Rev. Mod. Phys.*, 2013, **85**, 529.

44. H. Zhang, Z. Guo, H. Gao and T. Chang, *Carbon*, 2015, **94**, 60.

Table of contents entry

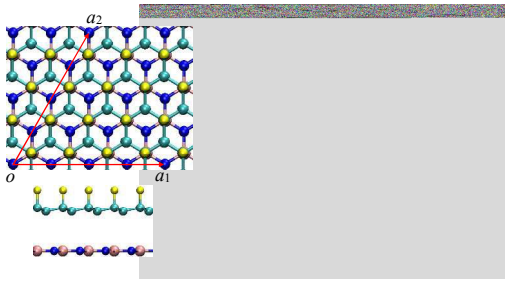

Surface functionalization can control and reduce the interfacial friction in commensurate graphene/h-BN heterostructure.